

RESEARCH PAPER

NiFe₂O₄@SiO₂@HKUST-1 as Novel Magnetic Metal-Organic Framework Nanocomposites for the Curcumin Adsorption

Mehrnaz Gharagozlou

Department of Nanomaterials and Nanocoatings, Institute for Color Science and Technology, Tehran, Iran

ARTICLE INFO

Article History:

Received 19 November 2021

Accepted 11 March 2022

Published 01 April 2022

Keywords:

Adsorption

Ferrite

Curcumin

Magnetic nanocomposites

Metal-organic framework

ABSTRACT

In this study, magnetic metal-organic framework nanocomposites $x(\text{NiFe}_2\text{O}_4)@(100-x)\text{SiO}_2@\text{HKUST-1}$ ($10 \leq x \leq 60 \text{wt.}\%$) were synthesized by an in-situ self-assembled method which is one of the green synthesis methods. Synthesized samples were characterized and their interaction with curcumin were investigated in aqueous solution. Phase formation, type of bonds formed, appearance and size of crystals, magnetic property and size of the specific surface area analyzed by X-ray diffraction (XRD), scanning electron microscopy (SEM), vibrating sample magnetometer (VSM) and BET surface area respectively. Results showed as the weight ratio of ferrite nickel to the silica substrate increases, the magnetic saturation increasing. By increasing the weight percentages of nickel ferrite from 10 to 50%, the BET surface area increases and pore volume decreases. Finally, the adsorption and interaction of curcumin and effective parameters such as drug and adsorbent dose on adsorption rates were investigated. Results showed the highest adsorption value (94%) was obtained for magnetic metal-organic framework nanocomposite (30% by weight) at pH=7, ambient temperature, contact time of 8 hours and with the weight ratio (2:1) of curcumin to synthesized magnetic metal-organic framework nanocomposite. Experimental data were better matched with Frondelich's adsorption isotherm. Although synthetic studies have shown that the process of adsorption and interaction of curcumin with a synthesized magnetic metal-organic framework nanocomposite, follows the quasi-second-order model.

How to cite this article

Gharagozlou M. NiFe₂O₄@SiO₂@HKUST-1 as Novel Magnetic Metal-Organic Framework Nanocomposites for the Curcumin Adsorption. J Nanostruct, 2022; 12(2):455-473. DOI: 10.22052/JNS.2022.02.020

INTRODUCTION

The drug curcumin scientifically known as diphtheria methane and is one of the main elements of the turmeric plant which belongs to the ginger family. In addition to curcumin, turmeric contains other compounds such as curcuminoid, cyclocurcumin, dimethoxy

curcumin and bisdemethoxycurcumin. Curcumin was first extracted in impure from the Curcuma Longa plant in 1815 and called curcumin [1-4]. Curcumin is a multifaceted molecule and has many therapeutic effects. Careful research over the past decade has proven the effectiveness of curcumin as an antioxidant, anti-inflammatory, anti-diabetic

* Corresponding Author Email: gharagozlou@icrc.ac.ir



and anti-arthritis [5, 6]. Its hydroxy groups are for antioxidant activity and methoxy groups are for anti-inflammatory and anti-proliferative activities. Curcumin has been used in traditional medicine for thousands of years, as well as in food coloring. Although there are different reports and opinions about the therapeutic benefits of curcumin, researchers should be careful because it is an unstable chemical [7].

It is insoluble in water but dissolves easily in solvents such as ethanol, acetone and methanol [8]. The only limiting factor in the use of this substance is its low solubility and low stability in the body. Curcumin is difficult to dissolve in water and is highly sensitive to changes in body pH. In addition, its adsorption through the gastrointestinal tract and in acidic environments is very low and after consuming it, the liver destroys a high amount of it [9]. Therefore, drug delivery systems based on nanotechnology, due to their potential characteristics and other unique properties, nanoparticles change the pharmacokinetics of the drug and also greatly improve the life of the drug in the bloodstream and the therapeutic properties of the drug. A group of nanoparticles is porous metal-organic framework (MOF) materials that synthesized in various types and considered by researchers due to various applications such as gas storage and separation, catalyst, sensor and drug storage and release [10-18].

Therefore, the metal-organic framework can be used in applications such as gas sensing [19], drug storage and release [20], catalysis [21] and drug adsorption due to their high specific surface area and porosity. Functionalization of zirconium-based metal-organic frameworks for gas sensing applications has been reported [19]. Among the porous nanoparticles of the metal-organic framework, magnetic metal-organic framework have received great attention in recent decades. Magnetic metal-organic framework are crystalline and porous materials and structure consist of metal clusters, organic ligands, and magnetic nanoparticles [22-24]. The metal ions of the coordination centers and ligands are also the link between the metal centers and the magnetic particles. Different metal-organic frameworks have been used to adsorb and interact with drugs. For example, Dong et al. synthesized and characterized the metal-organic framework (UiO-66) based on Zn and Hf by the macro method. They used the synthesized metal-organic framework as

an adsorbent for the drug curcumin and achieved an adsorption capacity of more than 450 mg/g for each one [14].

Prince et. al. synthesized the metal-organic framework (Ga-BDC) to adsorb the drug curcumin. They first synthesized and identified the desired metal-organic framework by microwave method and finally, to investigate the application of this metal-organic framework, it was used as an adsorbent for the drug curcumin [25]. Naseh et al. used a magnetic nanocomposite (FeNi₃/SiO₂/CuS) to adsorb and interact with the drug Metronidazole, which is an antibiotic and after examining the effective parameters of cysteine and isotherms, adsorption is studied. They found that the optimal conditions for adsorbing metronidazole is at pH=7, room temperature and 180 minutes [26].

Maggie et.al. used magnetic metal-organic framework adsorbents (Fe₃O₄/HKUST-1) to adsorb the fluoroquinolone antibiotics. They first synthesized and identified the magnetic metal-organic framework (Fe₃O₄/HKUST-1) by co-precipitation. Finally, to investigate the application of this synthesized magnetic metal-organic framework, they used it as an adsorbent of fluoroquinolones and studied isothermal and kinetic studies [27, 28]. TiO₂@SiO₂@NiFe₂O₄ magnetic nanocomposite has been also reported as catalyst for direct amide synthesis reactions [29]. Ni_{0.5}Zn_{0.5}Fe₂O₄ microtubes have been used for application as catalyst support in RF heated reactors [30]. However, no report has been published on the synthesis and use of the magnetic metal-organic nanocomposite (x(NiFe₂O₄)@(100-x)SiO₂@HKUST-1 (10≤x≤60wt.%)) to adsorb the drug curcumin. Therefore, the aim of this project is to synthesize and identify the magnetic metal-organic framework nanocomposite (x(NiFe₂O₄)@(100-x)SiO₂@HKUST-1) with different weight ratios of nickel ferrite to silica substrate and study their application in the process of uptake and drug interaction of curcumin. The next step is to investigate the type of nanocomposite and suitable magnetic metal-organic framework as a better adsorbent and also to find effective parameters for optimal adsorption and study conditions of isothermal and kinetic adsorption.

MATERIALS AND METHODS

Materials

In this study, all chemicals used were of

analytical grade and were used as received. Salts of iron nitrate (Fe(NO₃)₂·9H₂O), nickel nitrate (Ni(NO₃)₂·6H₂O) and copper nitrate (Cu(NO₃)₂·3H₂O) as metal precursors and the organic matter trichloroacetic acid (BTC) as the organic binding agent in the metal-organic framework were used. Also, tetraethyl ortho silica (TEOS) were used as a substrate for magnetic particles, 3-aminopropyl triethoxysilane were used as an amine agent, ethanol and water as solvents were used in synthesis. The water used were distilled water, and the curcumin aqueous solution were used as a drug as well as an oral dye to investigate its interaction and adsorption on the synthesized adsorbent. It should be noted that all the raw materials used, made by the German company Merck. By keeping the percentage of the metal-organic framework (HKUST-1) constant, the silica substrate was prepared by the weight ratio of 10, 30 and 50 percent on the nickel ferrite magnetic composite.

The formed phases and crystal structure of the synthesized metal-organic framework nanoparticles examined using X-ray diffraction (XRD, Philips) device equipped with copper lamp (Cu-Kα) and to detect the phases and sizes of nanoparticles crystals of magnetic metal-organic framework nanocomposite composites from X'Pert software and standard scatter plot (JCPDS) was used to compare and match the peaks obtained. External structure and geometric shape of magnetic metal-organic framework nanocomposite, phase differences and changes in nanocomposite it were studied by type MIRA3 field emission scanning electron microscopy (SEM) device made by TE-SCAN company. The magnetic properties of the synthesized metal-organic framework nanocomposites were performed using the vibrational magnetometer analysis (VSM) by the LBKFB device. Specific surface area measurement was performed according to the BET method and by analyzing the measurement of porosity and effective surface area (BET) using a device (Belsorp mini II from Microtrac Bel Corp company of Japan).

Synthesis of nickel ferrite in silica matrix x(NiFe₂O₄)@(100-x)SiO₂

The synthesis method of magnetic nickel ferrite nanocomposite in a silica matrix is in accordance with the method reported in the sources [31]. Nickel ferrite has wt.% of 10, 30, and 50 percent to

the 90, 70 and 50 weight percent of silica substrate respectively.

In this method, the nickel nitrate and iron nitrate were weighed in the amount of 6 and 9 g respectively, and dissolved in 10 ml of deionized water under reflux conditions and stir well with a mechanical mixer for 30 minutes to mix thoroughly. Next step, pour 60 ml of tetraethyl ortho silica (TEOS) into 50 ml of ethanol and 10 ml of water and acidify its pH using hydrochloric acid, and then pour it into the decanter and add it drop by drop to the solution inside the balloon and allow to stir for 2 hours for further mixing. In the third step, the contents of the balloon are poured into the crystallizer and placed slightly in the exposure of air for 7 days, and the alcogel is obtained. After 7 days, place the resulting alcogel in an oven at 110 °C for 24 hours to allow it to dry and xerogel obtain. The xerogel were calcined for 2 hours in an oven at 800 °C with a heating rate of 10 °C/min and the product were milled by a satellite mill.

Synthesis of magnetic nanocomposites x(NiFe₂O₄)@(100-x)SiO₂@HKUST-1

Dispense 1 g of nickel ferrite prepared in the previous section (2.2) with 50 ml of ethanol then add 2 ml (3-aminopropyl triethoxysilane) and under reflux conditions at 80 °C for 6 hours, allow to mix thoroughly and resulting sediment was separated using a magnet.

Pour 1 gram of the resulting powder with 25 mmol of copper nitrate, 22.5 mmol of lycopene tritactic acid (BTC) and 60 ml of distilled water in the balloon and re-mixed under reflux conditions at 100 °C for 8 hours. After washing, the resulting deposit was placed in a vacuum oven at 120 °C for 10 hours to allow the precipitate to dry and the magnetic metal-organic framework nanocomposites (x(NiFe₂O₄)@(100-x)SiO₂@HKUST-1) formed.

Preparation of curcumin solution

The tested curcumin powder was first dissolved in 10 ml of pure ethanol and then solution diluted using deionized water. The amount of curcumin was calculated according to its mass and purity, and accordingly, the available solution for the study was made with different concentrations in a volume of 500 ml, and finally, 100 ml of it was considered as a statistical population.

Investigation and study of the curcumin adsorption

process

To investigate the process of adsorption of curcumin solution on the synthesized adsorbents, 100 ml of the curcumin solution was taken as a sample and the adsorbent was added to it and placed on the shaker at room temperature for 2 hours. After a while, the sample was taken and centrifuged for better separation. The concentration of curcumin solution in the samples taken at different times and were measured using a UV light spectrometer.

Finally, using equation (1), the adsorption percentage of curcumin solution and using equation (2), the adsorption capacity of the synthesized magnetic metal-organic framework nanocomposite was calculated and determined.

$$\% \text{Adsorption} = (C_0 - C_t / C_0) \times 100 \quad (1)$$

$$q_t = (C_0 - C_t) V / m \quad (2)$$

where C₀ and C_t are the initial concentration of curcumin solution and the concentration of curcumin solution at time t respectively, V is the volume of curcumin solution (Liter), m the amount of adsorbent (g) and q_t are the adsorption capacity of the magnetic metal-organic framework nanocomposite in terms of (mg.g⁻¹) [32-35]. Finally, the effect of parameters such as adsorbent dose, adsorbent type and concentration of curcumin solution on the adsorption of curcumin solution by synthesized magnetic metal-organic framework nanocomposites was studied.

To investigate the behavior of the synthesized adsorbent, the relationship between the adsorbing sample and the adsorbent surface and sample interaction with the adsorbent requires the equations that are used to investigate this adsorption behavior. There are several ways to look at adsorption isotherms. These isotherms include the Langmuir, Freundlich and the Temkin. In this study, two isotherms of Langmuir and Freundlich with the following equations have been used to investigate the ruling isotherm to the adsorption process [35-37].

The Langmuir adsorption isotherm model is examined and calculated with equation 3 and its variables are presented in Table 5. The Langmuir adsorption isotherm is based on the single-layer adsorption of the adsorbent, which here is the curcumin solution, on the adsorbent surface, indicating that no reaction occurs between the

adsorbed sample and adsorbent molecules.

$$C_e / q_e = 1 / K_L \cdot q_L + C_e / q_L \quad (3)$$

in this equation, C_e is the concentration of curcumin solution at equilibrium (mg.l⁻¹), q_e is the amount of material adsorbed per unit mass of the adsorbent, q_L the maximum adsorption capacity is synthesized on the nanocomposites of the magnetic metal-organic framework, and K_L is the Langmuir constant which refers to the energy of adsorption.

The Freundlich isotherm model is examined and calculated with equation 4 and its variables are presented in Table 5. Frondelich adsorption isotherm is synthesized on the adsorbent based on multi-layered and heterogeneous adsorption of the adsorbent. The closer value of 1/n to zero showing more heterogeneous adsorption and if the value is 0.1 > 1/n > 1, the adsorption process is optimal [38].

$$\text{Ln } q_e = \text{Ln } K_F + (1/n_F) \text{Ln } C_e \quad (4)$$

In the above relation C_e the concentration of curcumin solution at equilibrium (mg.l⁻¹), q_e the amount of material adsorbed per unit mass of the adsorbent, 1/n the heterogeneous factor that indicates the type and severity of adsorption and K_F is the constant isotherm of the Frondelich.

The third isothermal model studied is Temkin isotherm with linear equation 5, this calculation model and its variables are presented in Table 5.

$$q_e = B_1 \text{Ln } K_T + B_1 \text{Ln } C_e \quad (5)$$

In the above relation C_e the concentration of curcumin solution at equilibrium (mg.L⁻¹), q_e the amount of substance adsorbed per unit mass of the adsorbent, K_T isotonic adsorption coefficient of Temkin and B₁ is the slope of the diagram of this isotherm [38-42].

Adsorption kinetics is used to determine the mechanism and rate of the kinetic of the synthesized magnetic metal-organic framework nanoparticle and to control the adsorption processes [43]. There are several different kinetic models used in this study to better understand the experimental data of the process of adsorption of curcumin solution by magnetic metal-organic framework nanocomposite synthesized from quasi-first and second-order kinetics and intramolecular penetration to quantify the quantitative adsorption

kinetics. The quasi-first-order model occurs with an equation of 6 expressing penetration into the single layer, and the changes in adsorption value over time are proportional to the number of unoccupied adsorbent sites [44-46].

$$\ln (q_e - q_t) = \ln q_e - k_1 t \quad (6)$$

In equation 6, K_1 equilibrium constant quasi-first order velocity (min⁻¹), q_e the amount of curcumin adsorbed in equilibrium (mg/g) and q_t is the amount of curcumin adsorbed at time t (mg/g). The quasi-second order model with Equation 7 represents the chemical adsorption rate with a slowing speed which controls surface adsorption where the square of the number of unoccupied sites in the adsorbent is proportional to the occupancy rate of the adsorbed sites [47].

$$t / q_t = 1 / K_2 q_e^2 + t / q_e \quad (7)$$

In this regard, K_2 is the equilibrium constant of the second-order kinetic and in terms of (g/mg .min). The parameters q_e and q_t indicate the

amount of curcumin adsorbed in equilibrium and the amount of curcumin adsorbed at time t and in terms of (mg/g) respectively. Finally, by comparing these three kinetic models, it can be estimated which synthesized metal-organic framework nanocomposite follows which kinetics model and its adsorption rate are calculated [48-51].

RESULTS AND DISCUSSION

Characterization of synthesized magnetic metal-organic framework nanocomposite

The synthesized magnetic metal-organic framework nanocomposite with different weight ratios from ferrite nickel and silica substrate was characterized by analyzes SEM, TEM, XRD, VSM and BET.

Fig. 1a shows the image of the electron microscopy associated with NiFe₂O₄@SiO₂. Observations indicate that the uniformly dispersed, well crystallized and almost spherical Ni-ferrite nanoparticles were homogeneously embedded in the silica network with the average particle sizes of 14 nm. Spherical NiFe₂O₄ nanoparticles homogeneously dispersed in the silica matrix.

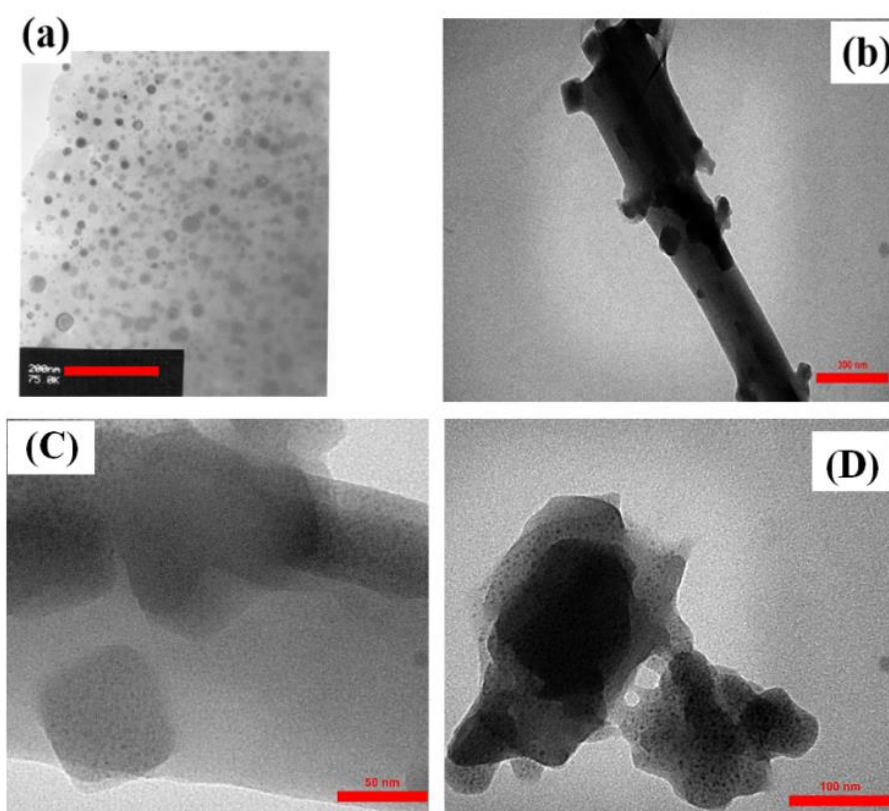


Fig. 1. TEM analysis image of (a) $x(\text{NiFe}_2\text{O}_4)@(100-x)\text{SiO}_2$, $x=30$ and magnetic metal-organic framework nanocomposite $x(\text{NiFe}_2\text{O}_4)@(100-x)\text{SiO}_2$ @HKUST-1 (b) $x=30$, (c) $x=10$, (d) $x=50$

Higher silica weight ratio resulted in lower particle size of NiFe_2O_4 nanoparticles.

Fig. 1(b-d) shows the image of the electron microscopy associated with the magnetic metal-organic framework nanocomposite $((x\text{NiFe}_2\text{O}_4)_@ (100-x)\text{SiO}_2@ \text{HKUST-1}$ $x=30, 10, 50$) synthesized in this study with magnification KX200. According to the images, the metal-organic framework nanocomposite were almost rod-shaped with the thickness of about 200 nm, and the nickel ferrite were dispersed inside and outside the silica substrate with the particle size of 80, 50 and 30 nm for $x=30, 10$ and 50, respectively.

SEM image of $\text{NiFe}_2\text{O}_4@ \text{SiO}_2$ (Fig. 2a) shows spherical agglomeration. SEM of the synthesized magnetic metal-organic framework shows that these nanocomposites have rod morphology (Fig. 2b). The nickel ferrite nanoparticles in the silica matrix are placed side by side in such a way that they form a rod structure and the HKUST-1 metal-organic framework is placed on them. It has also

been shown that the synthesized nanocomposite is hollow and has a crystalline and dense structure [52].

The X-ray diffraction analysis was used to investigate the formed phases and the structure of the synthesized magnetic metal-organic framework nanocomposites and to calculate the size of the crystals. Fig. 3 shows the XRD diagram of the synthesized samples.

The crystal structure of metal-organic framework (HKUST-1) at 2θ has index peaks at 20.66° , 15.92° and 13.65° , as well as the presence of index peaks at $20-35^\circ$ related to nickel ferrite and the presence of silica in the nanocomposite. Peaks at the $40-55$ degree range are due to the presence of nickel ferrite in the silica substrate, indicating that the xerogel amorphous nickel ferrite is located in the silica matrix. Finally, the Scherrer equation was used to calculate the crystal size of the synthesized magnetic metal-organic framework. Crystal sizes obtained from equation

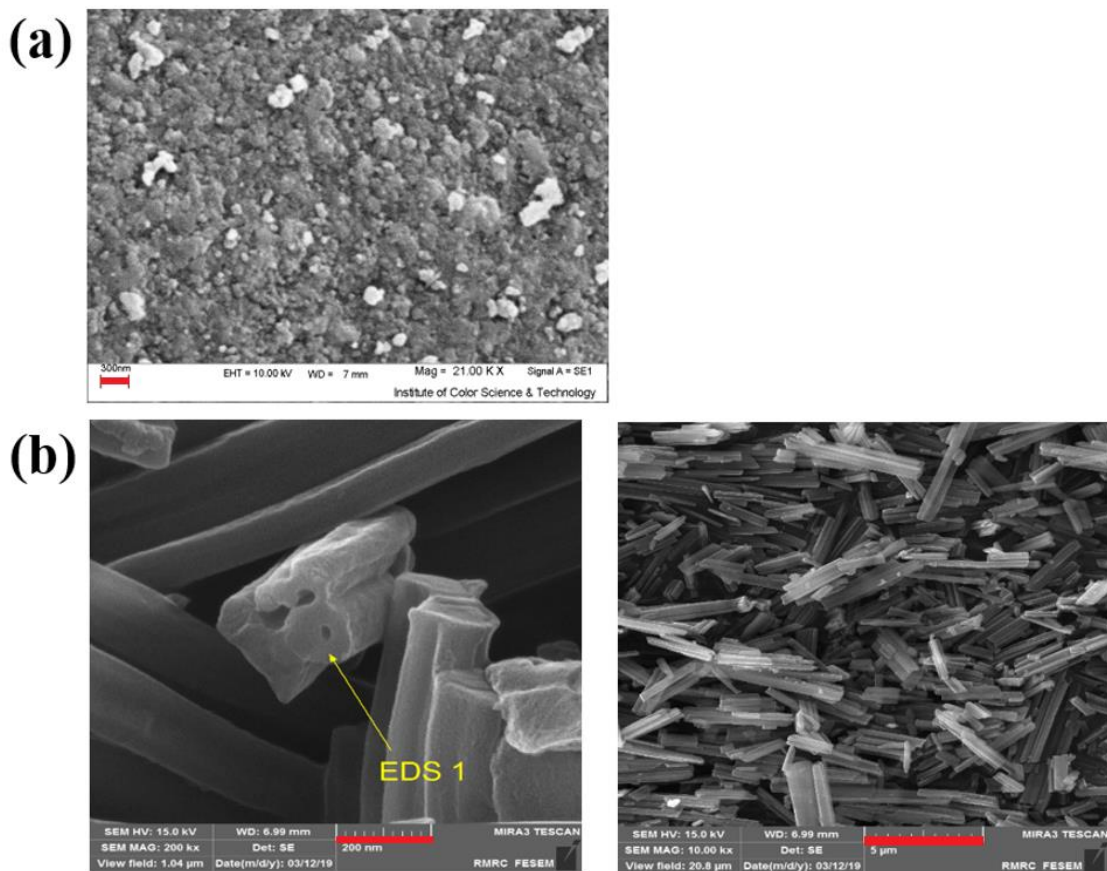


Fig. 2. Image analysis of SEM analysis of (a) $x\text{NiFe}_2\text{O}_4@(100-x)\text{SiO}_2$ $x=30$, (b) magnetic metal-organic framework nanocomposite $x\text{NiFe}_2\text{O}_4@(100-x)\text{SiO}_2@ \text{HKUST-1}$ $x=30$

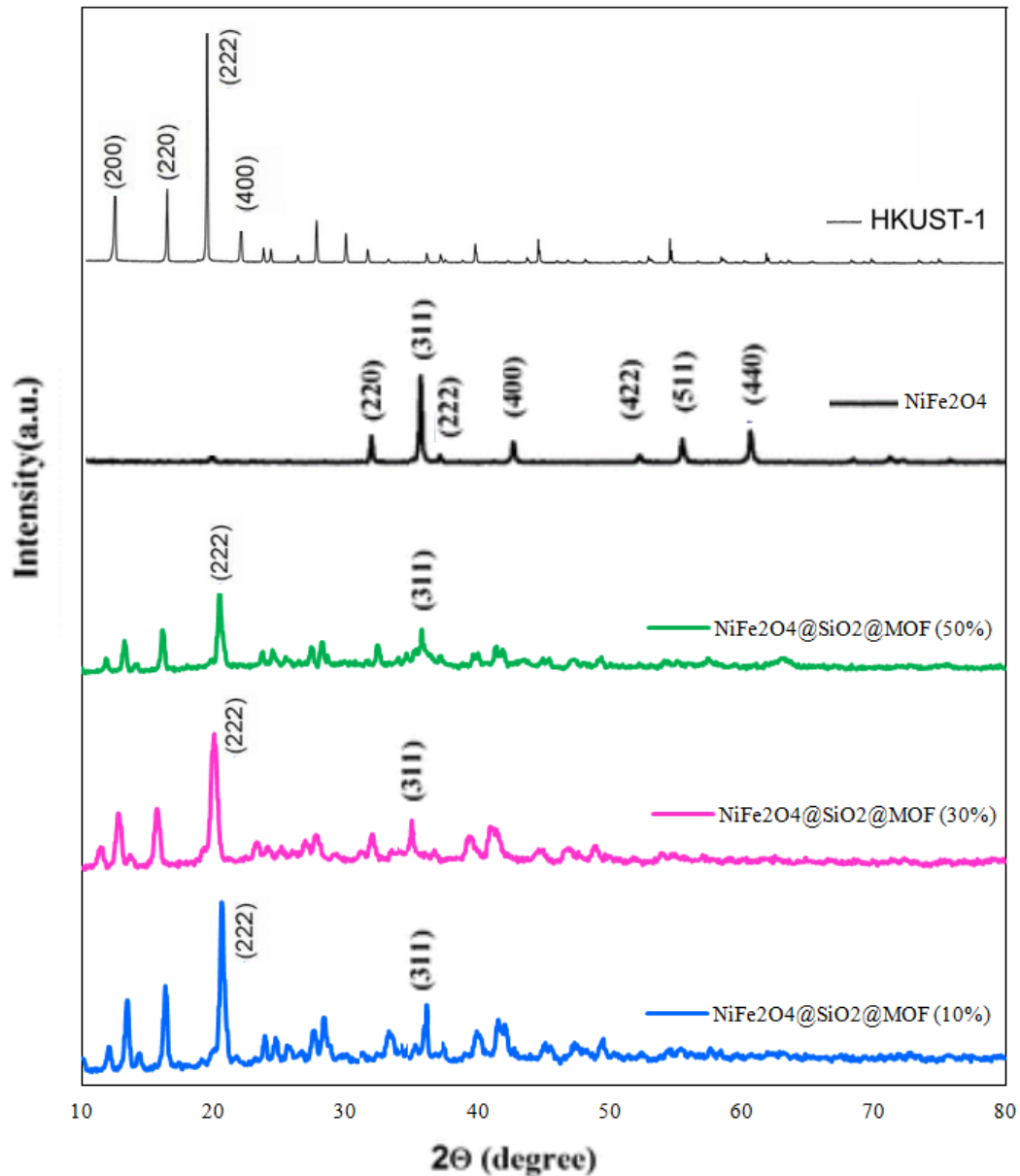


Fig. 3. XRD diagram of magnetic metal-organic framework, nickel ferrite and magnetic metal-organic framework nanocomposite synthesized with different nickel ferrite percentages

(8) showed that the higher ratio of nickel ferrite to the silica matrix led to the larger nanocomposite. In Table 1, the crystal sizes for synthesized magnetic metal-organic framework nanocomposites are calculated and presented.

$$D = b \lambda / \beta \cos \theta \quad (8)$$

In this regard, D diameters of nanocomposites, b is a constant, which normally takes a value

between 0.89 and 0.94 depending on the function used to fit the peak, λ is the X-ray wavelength irradiated, β is the peak width at half height or FWHM, which should be placed in the formula according to radians and θ is the peak location on the horizontal axis of the scatter pattern [11].

The synthesized metal-organic framework nanocomposites were examined using VSM analysis at ambient temperature to investigate the magnetic properties. Fig. 4 shows the VSM magnetic

Table 1. Crystal parameters of synthesized magnetic metal-organic framework nanocomposites

Sample	Peak pos. [$^{\circ}2\theta$]	Crystallite size [nm]	d-spacing [nm]
(xNiFe ₂ O ₄)@(100-x)SiO ₂ @HKUST-1 x=10)	19.909	20.5	4.45
(xNiFe ₂ O ₄)@(100-x)SiO ₂ @HKUST-1 x=30)	20.627	32.8	4.30
(xNiFe ₂ O ₄)@(100-x)SiO ₂ @HKUST-1 x=50)	20.467	41.0	4.33

analysis diagram for the synthesized magnetic metal-organic framework nanocomposites.

The magnetized curves of the synthesized samples show that the synthesized magnetic metal-organic framework nanocomposites having a good superparamagnetic property with different magnetic saturation. In magnetic metal-organic framework nanocomposites, as the weight ratio of

ferrite nickel to the silica substrate increases, the magnetic saturation increasing. The parameters obtained from this analysis are presented in Table 2. Therefore, it can be concluded that, studied metal-organic framework nanocomposites are easily dispersed in water and can be collected by an external magnetic field [29, 30, 53-55].

Accurate measurement of surface area

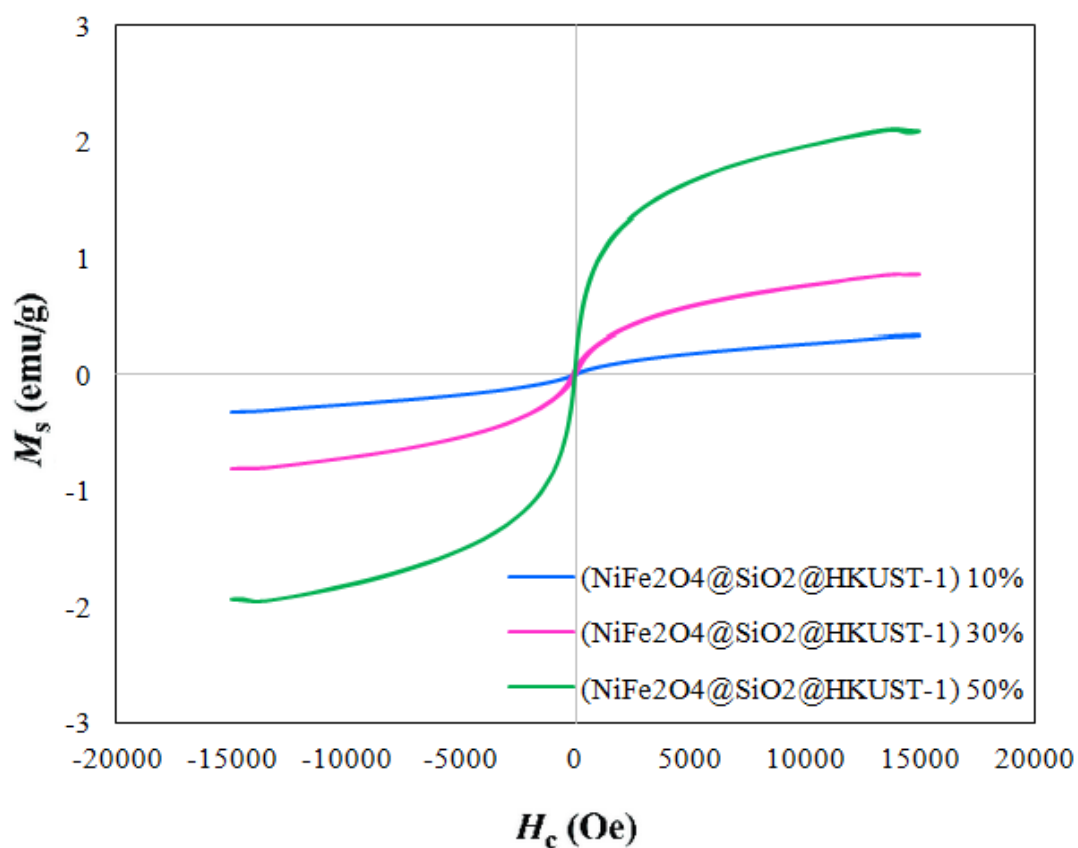


Fig. 4. VSM analysis of synthesized magnetic metal-organic framework nanocomposites

Table 2. VSM analysis parameters for synthesized metal-organic framework nanocomposites.

Sample	M _r [emu/g]	M _s [emu/g]	H _c [Oe]
x(NiFe ₂ O ₄)@(100-x)SiO ₂ @HKUST-1 x=10	0.0039	0.34	0.003
x(NiFe ₂ O ₄)@(100-x)SiO ₂ @HKUST-1 x=30	0.016	0.87	0.04
x(NiFe ₂ O ₄)@(100-x)SiO ₂ @HKUST-1 x=50	0.11	2.09	0.1

and material porosity is important in many applications, such as nano sorbent for the metal-organic framework and metal nanoparticles. Therefore, using BET analysis, the type of porosity, surface area and diameter of pores in synthesized magnetic metal-organic framework nanocomposites can be measured. In the range of the BET equation validity (generally 0.1 - 0.3 relative pressure) there should be no difference between adsorption and desorption branches, this hysteresis is due to mesopores filling and emptying processes and occurs at higher relative pressures. Pore size is not to be determined from BET analysis. BET is in a strict sense just used for calculation of surface area in a non-porous surface (from BET calculation you will obtain the amount of adsorptive that will cover a monolayer), although it is widely accepted to be used as a reference for porous samples, even if the non-porous filling mechanism is not the most physically correct.

Table 3 presents the BET analysis parameters for the synthesized magnetic metal-organic framework nanocomposites with different percentages of ferrite nickel to the silica matrix.

Based on Table 3 results, by increasing the percentages of nickel ferrite from 10 to 50%, the BET surface area increases and pore volume decreases. These pores, which are only due to the

presence of the HKUST-1 metal-organic framework, are not uniform in pores diameter because the ferro-nickel nanocomposites are non-dispersed. Also, as the percentage of nickel ferrite, which is the same as the heavy nuclei in the silica bed, increases, these pores fill and the pore volume decreases [34]. According to SEM images and BET analysis, the synthesized magnetic metal-organic framework nanocomposite is a porous material and since the pore diameter of these nanocomposites is bigger than 4 nm, they are in the category of mesoporous materials. These pores, which are only due to the presence of the HKUST-1 metal-organic framework, are not uniform in diameter because nickel ferrite nanocomposites are non-dispersed in them. Therefore, as the percentage of nickel ferrite, which is the heavy nuclei in the silica bed, increases, these pores fill and the pore volume decreases [34].

Adsorption optimization tests

Investigating effect of magnetic metal-organic framework nanocomposite dose on curcumin uptake

To investigate the effect of the interaction of curcumin molecules with magnetic metal-organic framework nanocomposite, prepared the aqueous solution of curcumin with a concentration

Table 3. BET analysis parameters for the synthesized magnetic metal-organic framework nanocomposites with different percentages of ferrite nickel to the silica matrix.

Sample	BET (m ² /gr)	Pore volume (nm)	Pore type
x(NiFe ₂ O ₄)@(100-x)SiO ₂ @HKUST-1 x=10	378.7	7.28	Mesoporous
x(NiFe ₂ O ₄)@(100-x)SiO ₂ @HKUST-1 x=30	433.8	6.99	Mesoporous
x(NiFe ₂ O ₄)@(100-x)SiO ₂ @HKUST-1 x=50	898.4	5.14	Mesoporous

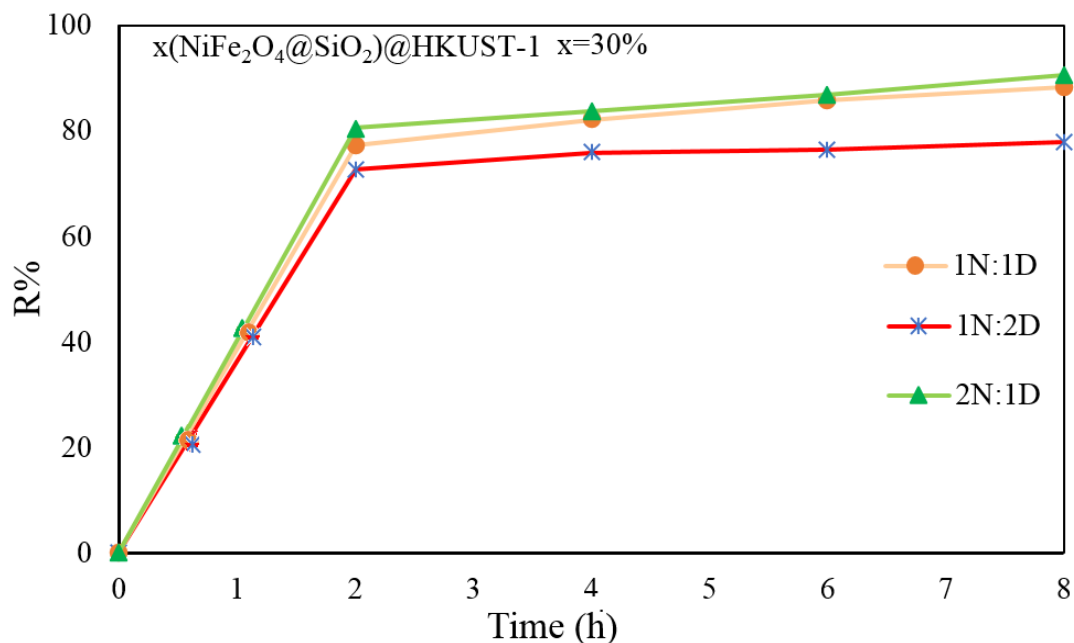


Fig. 5. Investigation of the effect of nanocomposite concentration on curcumin

(100 ppm) and then 100 ml of solution were sampled. The accurate amount of curcumin in solution was added to various ratios of (1:2), (2:1) and (1:1) magnetic metal-organic framework nanocomposites $(x(\text{NiFe}_2\text{O}_4)@(100-x)\text{SiO}_2@$ HKUST-1 $x=30$). Put the solution on the shaker for better mixing. Sampling and centrifugation performed every 2 hours and spectrophotometer used to measure the wavelength and the adsorption value was calculated.

Fig. 5 showed, as the nanocomposite ratio of the magnetic metal-organic framework to curcumin increases, the adsorption efficiency increases. It was also obtained that the maximum efficiency (90%) were reached after 8 hours when the nanocomposite of the magnetic metal-organic framework of the magnet was double of the amount of curcumin used in the solution. This increase in efficiency is due to the increase in sites and free pores due to the increase in the concentration of metal-organic framework nanocomposite compared to the concentration of curcumin in the solution.

Investigation effect of type of magnetic metal-organic framework nanocomposite on curcumin uptake

First made a 10 mg/L solution of curcumin and

sampled 100 cc of it. Synthesized magnetic metal-organic frameworks HKUST-1 with different weight percentages and NiFe₂O₄@SiO₂ nanocomposites as adsorbents in a ratio of (2:1) and the drug added to 100 cc curcumin solution sample. Then it was placed on the shaker at room temperature. As in the previous step, sampling and adsorption amounts were calculated.

The results showed in Fig. 6, the magnetic nanocomposite (NiFe₂O₄@SiO₂) adsorbed 73% after 8 hours. This value was less than the adsorption of curcumin by metal-organic framework nanocomposites $(x(\text{NiFe}_2\text{O}_4)@(100-x)\text{SiO}_2@$ HKUST-1 $x=30$) and under the same conditions, metal-organic framework nanocomposite adsorbed 78.45% after 8 hours. After 8 hours, these particles were homogeneous in curcumin solution and could not be separated. Over a period of 8 hours, magnetic nanocomposite containing a metal-organic framework with a 30 %wt weight higher percentage showed the highest adsorption value (94%). According to the obtained results, for further investigation, magnetic metal-organic framework nanocomposite with a weight percentage of 30% wt. were used as an optimum percentage.

As shown in Table 4, based on the obtained results and comparison with other metal-organic

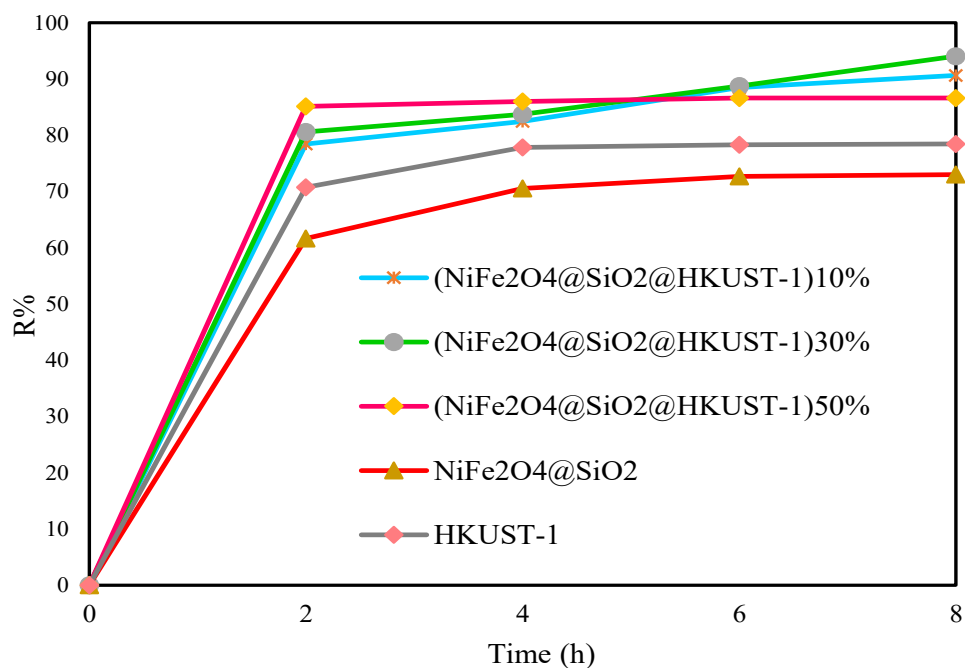


Fig. 6. Effect of different percentages of containing metal-organic framework nanocomposite and Nickel ferrite nanocomposite on the silica substrate on adsorption.

frameworks, it can be concluded that magnetic metal-organic framework nanocomposite, like other metallic organic frameworks, is a viable option for uptake and drug interaction of curcumin.

Investigating the effect of curcumin solution concentration on adsorption

To investigate the effect of curcumin concentration, first curcumin solutions with concentrations of 10, 30 and 50 ppm were

prepared. As in the previous steps, the optimal amount of adsorbent was added to it and placed on the shaker at room temperature. Every 2 hours, it was sampled, centrifuged and sample wavelength was measured using a spectrophotometer.

The results in Fig. 7 indicated, higher concentration of curcumin drug solution led to lower adsorption efficiency. It was also obtained curcumin solution at the highest concentration (ppm10) showed the highest adsorption

Table 4. Evaluation of curcumin adsorption capacity, contact time of 8 hours, on various metal-organic framework nanocomposites

MOF	Surface area (m ² g ⁻¹)	Adsorbed	Adsorption Capacity (mg/g)	Ref
UiO-66	1398		34.5	[57]
Hf- UiO- 66	950		463.02	[14]
Zr- UiO- 66	1400		466.39	[14]
Zr- UiO- 66ST	1276		393.22	[57]
Ca-BDC	792	Curcumin	140	[22]
NiFe ₂ O ₄ @SiO ₂ @HKUST-1	898		358	This study

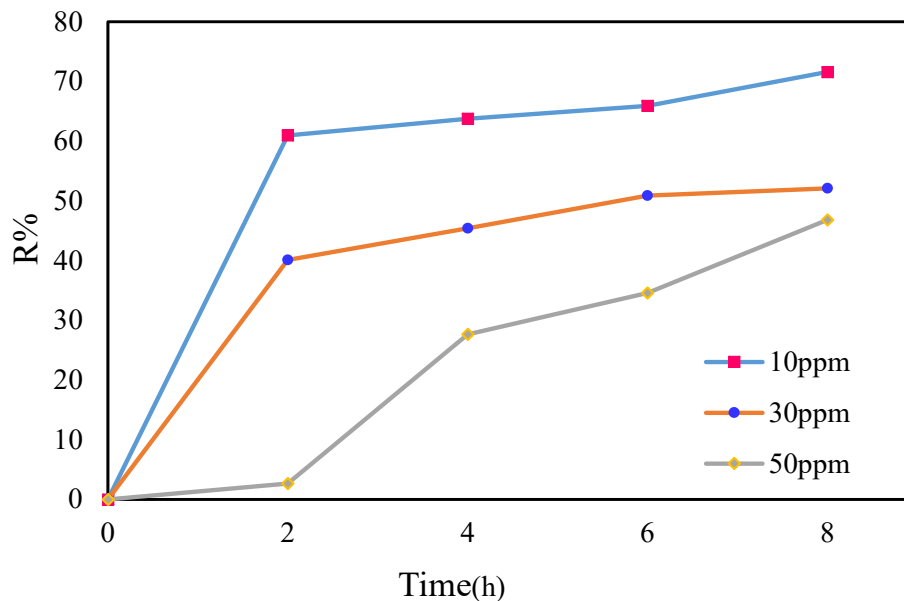


Fig. 7. Investigation of the effect of curcumin drug concentration on adsorption.

efficiency because at this concentration the amount of curcumin in the solution is less than the concentration of 30, 50 and resulted, specific surfaces, empty pores and many active sites still exist in the nanocomposite surface of the metal-organic framework that is not saturated and increases the efficiency of the metal-organic framework nanocomposite adsorption.

Curcumin adsorption kinetics study

To check the adsorption rate, kinetic adsorption and interaction behavior between curcumin and synthesized metal-organic nanocomposites with weight percentages 30, 10 and 50, three kinetic models of first-order, second-order and intra-molecular adsorption were used (Fig. 8). The kinetic variables of the surface adsorption process of curcumin by the magnetic metal-organic framework nanocomposites studied and presented in Table 5.

The quasi-second order were found to be better than the other two models for synthesized magnetic metal-organic frameworks nanocomposites because of the above equation, the R^2 correlation coefficient for the quasi-second order is calculated. All coefficients are very close to one, while the two models of the quasi-first order and the intra-molecular diffusion, are more distant from the quasi-second order model, respectively.

So we can conclude curcumin adsorption kinetics

using a variety of synthesized nanocomposites follows the quasi-second order. On the other hand, the amount of (q_e) Cal adsorption obtained from the above equations in the kinetic model adsorption is quasi-secondary order it is much closer to the experimental adsorption of (q_e) exp.

Among the synthesized nanocomposites, metal-organic framework nanocomposite (NiFe₂O₄@SiO₂@HKUST-1) with a 30% weight percentage showed better adsorption. As a result, the kinetics of adsorption for this metal-organic framework nanocomposite are calculated in different concentrations of curcumin solution. To find the kinetic adsorption of this nanocomposite, all three models mentioned above were examined.

Study of isothermal adsorption models

In this study, to evaluate the isotherms of adsorption on the desired adsorbent under optimal conditions, the three adsorption isotherms of Langmuir, Freundlich and Tamkin were examined (Fig. 9).

In isothermal adsorption, it is assumed that the drug is placed on the adsorbent as a single-layer coating. According to the calculation, the R^2 obtained from the isotherm is the adsorption of Langmuir (0.948), which indicates that there is a single molecular adsorption of curcumin on the target adsorbent.

Freundlich adsorption isotherm is widely

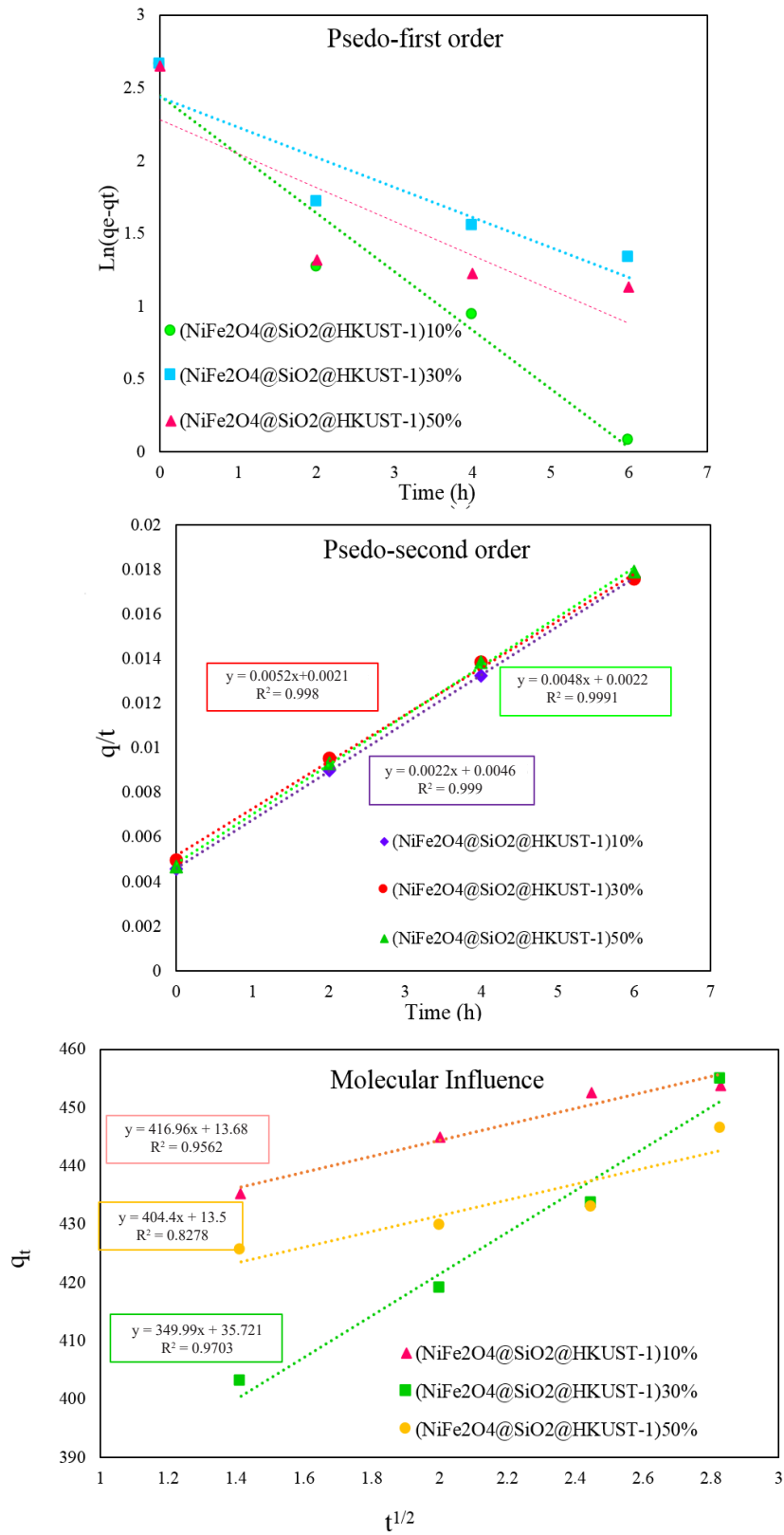


Fig. 8. Investigation of kinetic adsorption models

Table 5. Data obtained from the calculation of different synthetic adsorption models for different types of synthesized nanocomposites

Model	Parameter	Adsorbent		
		F-S-MOF10%	F-S-MOF30%	F-S-MOF50%
Pseudo First-Order	(q) _{ex}	453.78	454.95	446.5
	(q) _{cel}	139.63	272.897	190.1078
	K ₁	1.077	2.097	1.864
	R ²	0.942	0.838	0.7029
Pseudo Second-Order	(q) _{ex}	453.78	454.95	446.5
	(q) _{cel}	464.54	476.19	454.54
	K ₂	0.0161	0.0053	0.0121
	R ²	0.999	0.998	0.9991
Molecular Influence	K _p	161.93	160.16	157.29
	l	75.84	63.663	73.56
	R ²	0.8021	0.848	0.8024

used for multilayer adsorption modeling on heterogeneous adsorbent surfaces and it is not limited to the formation of a single layer on the surface in addition adsorption functions can also be described using the Freundlich isotherm parameters. As can be seen from the calculations, R² is obtained from the calculations of this isotherm (0.995). Also, the value (1/n) obtained indicates that the adsorption conditions of curcumin on the adsorbent are optimal and the curcumin groups are adsorbed on the heterogeneous adsorbent surface. Using the Temkin adsorption isotherm, the ratio of the surface covered to the total available surface can be obtained for the adsorbent and in this isotherm, R² is equal to (0.945). This indicates that almost a large area of the adsorbent is available to absorb curcumin and is covered with curcumin. Table 6 presents different types of isotherms of adsorption and their parameters.

According to the data in Table 6, the correlation coefficients (R²) of all three adsorption isotherms of Langmuir, Freundlich and Temkin and compliance are close to one, but the correlation coefficient of Freundlich adsorption is the highest. This indicates that the isotherm was the dominant isotherm of the Freundlich. This means that the adsorption process has been multi-layered on

heterogeneous surfaces, as a result, this model describes experimental data well. Therefore, the mechanism of adsorption of curcumin on the nanocomposite of the magnetic metal-organic framework and a filling of the available adsorbent surface of curcumin.

Adsorption thermodynamics

The thermodynamic parameters of the adsorption progress are calculated via the following equations (9) and (10) [58], respectively:

$$\ln q_e/C_e = \Delta S^\circ/R - \Delta H^\circ/RT \quad (9)$$

$$\Delta G^\circ = \Delta H^\circ - T \Delta S^\circ \quad (10)$$

where R is the gas constant (8.314 J mol⁻¹K⁻¹), ΔS° is the entropy change (J mol⁻¹K⁻¹), ΔG° is the free energy change (kJ mol⁻¹). From the plot and intercept of ln(q_e/C_e) versus 1/T thermodynamic parameters of adsorption on were obtained and listed in Table 7. The negative values of ΔG° indicated that the adsorption process was spontaneous within the temperature range evaluated. The negative enthalpy value of ΔH° indicated that the adsorption of this study was an exothermic

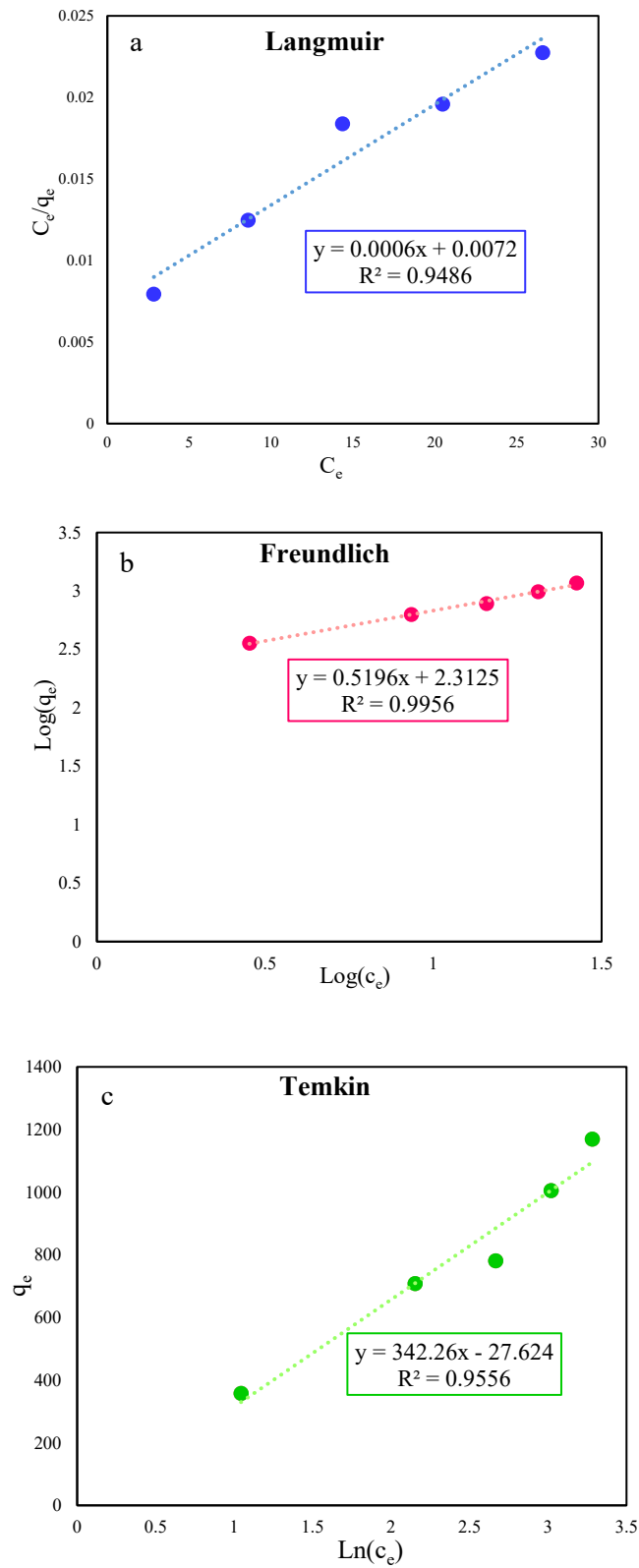


Fig. 9. Investigation of adsorption isotherms, a) Langmuir isotherm b) Freundlich isotherm c) Temkin isotherm.

Table 6. Different types of isotherms of adsorption and their parameters

Adsorbent		
Model	Parameter	F-S-MOF30%
		Concentration(mg/L) 30
Langmuir	(q) _{ex}	358
	(q) _m	222.330
	K _L	0.397
	R ²	0.948
Freundlich	(q) _{ex}	358
	K _F	370.37
	1/n	0.1045
	R ²	0.995
Temkin	K _T	124.64
	B ₁	45.706
	R ²	0.945

reaction. which was in accord with the decreasing adsorption capacity associated with increasing adsorption temperature. Also, the negative values of entropy (ΔS°) indicated that decreased randomness at the solid-solution interface of the adsorption on the nanocomposite surface.

The mechanism of adsorption of curcumin on x(NiFe₂O₄)@(100-x)SiO₂@HKUST-1

Based on the analysis of experimental data, the mechanism of adsorption of curcumin on the metal-organic framework nanocomposite adsorbent are attributed to (π - π) bonds, hydrogen bonds and electrostatic interactions between the

curcumin functional groups and the metal-organic framework (Fig. 10). The role of NiFe₂O₄ and SiO₂ can describes as the silica matrix network provides an ideal nucleation environment to uniformly disperse NiFe₂O₄ nanoparticles and thus to confine them to aggregate and coarsen. This porous and extended network is a good platform for formation the nanocomposite with metal organic framework. The obtained magnetic nanocomposite is smart due to its magnetic NiFe₂O₄ component dispersed in non magnetic SiO₂ matrix and can be easily controlled with a magnet.

These high adsorption capacities were obtained at pH=7, where curcumin molecules are natural or

Table 7. Thermodynamic parameters for the adsorption on nanocomposite surface with initial concentration of 100 mg/L

Nanocomposite	T (K)	ΔG° (kJ/mol)	ΔH° (kJ/mol)	ΔS° (J/mol K)
x(NiFe ₂ O ₄)@(100-x)SiO ₂ @HKUST-1 x=30	303	-12.01	-29.01	-49.09
	323	11.07		
	333	10.11		

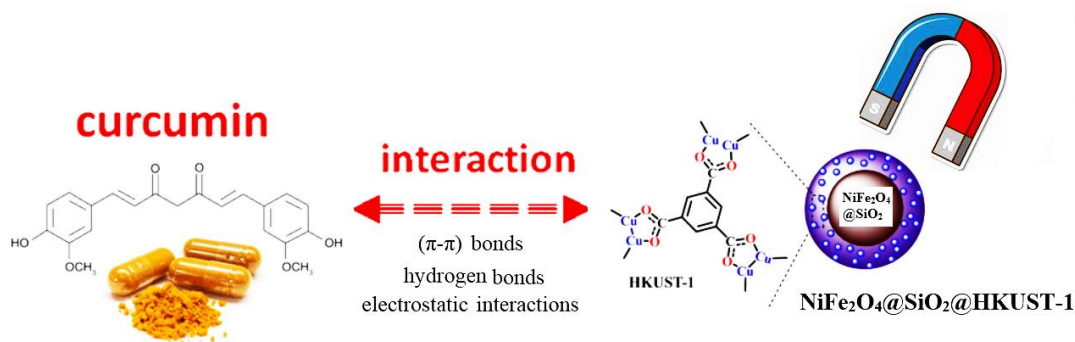


Fig. 10. Mechanism of adsorption of curcumin on $x(\text{NiFe}_2\text{O}_4)@(100-x)\text{SiO}_2@HKUST-1$

neutral. In addition, coordinate bonds have been established between Cu^{2+} open sites within the HKUST-1 metal-organic framework and CO- and O-groups in curcumin molecules. Hydrogen bonds are also formed between Cu-O-Cu molecules in HKUST-1 and OH in curcumin. On the one hand, curcumin molecules can form covalent bonds with the Si-O group in nanocomposites through silica-oxygen bonds in D-ketones [35,58,59]. On the other hand, curcumin binds strongly to most metal ions, because curcumin has acted as a ligand and are attached to the central metals that act as the core of the metal-organic framework and create stable complexes [60-63]. It is approved by using biocompatible nanomaterial for efficient curcumin loading [64,65].

CONCLUSION

Currently, the drug curcumin has been absorbed and examined using metal-organic framework nanocomposites. Magnetic metal-organic framework nanocomposites with ferrite nickel weight ratios of 30, 10 and 50 to silica matrix were synthesized by the in-situ self-arrangement method. Magnetic metal-organic frameworks nanocomposite with ferrite nickel ratio of 30% by weight to silica matrix acted as the best adsorbent with the highest capacity to absorb curcumin. The results of drug uptake and interaction by this nanocomposite showed a synthesized magnetic metal-organic framework in an environment with pH=7, contact time 8 hours, the dose of drug 10 ppm and the amount of adsorbent double of the dose of the drug are the optimum values for achieving the maximum adsorption capacity of the drug curcumin by magnetic metal-organic frameworks nanocomposite with a weighted ratio

of 30% of ferrite nickel to the synthesized silica matrix. The results showed that adsorption and drug interaction on the synthesized adsorbent with the isothermal model of Freundlich adsorption has a better match and most of the adsorption process is chemical. The process of drug uptake and interaction of curcumin follows second-order kinetics. Based on the obtained results, NiFe₂O₄@SiO₂@HKUST-1 magnetic metal-organic frameworks nanocomposite is a good option for absorbing and interacting with curcumin.

ACKNOWLEDGMENT

Author acknowledge the Institute for Color Science and Technology for cooperation and providing chemicals, materials, and characterization equipment to carry on this study.

CONFLICT OF INTEREST

The author declare that there is no conflict of interests regarding the publication of this manuscript.

REFERENCE

1. Ahmadi F, Valadbeigi S, Sajjadi SE, Shokoohinia Y, Azizian H, Taheripak G. Grandivittin as a Natural Minor Groove Binder Extracted From *Ferulago Macrocarpa* to ct-DNA, Experimental and In Silico Analysis. *Chem Biol Interact*, 2016; 258: 89-101.
2. Gosling C. Leung's Encyclopedia of Common Natural Ingredients: Used in Food, Drugs, and Cosmetics. (3rd edition), Ref Rev, 2010; 24(7): 42-43.
3. Kiuchi F, Goto Y, Sugimoto N, Akao N, Kondo K, Tsuda Y. Nematocidal Activity of Turmeric: Synergistic Action of Curcuminoids. *Chem Pharm Bull*, 1993; 41(9): 1640-1643.
4. Rodrigues JL, Prather KLJ, Kluskens LD, Rodrigues LR. Heterologous Production of Curcuminoids. *Microbiol Mol Biol Rev*, 2015; 79(1): 39-60.
5. Heger M, Golen RF, Broekgaarden M, Michel MC. The Molecular Basis for the Pharmacokinetics and

- Pharmacodynamics of Curcumin and Its Metabolites in Relation to Cancer. *Pharmacol Rev*, 2014; 66(1): 222-228.
6. Perrone D, Ardito F, Giannatempo G, Dioguardi M, Troiano G, LoRusso L, DeLillo A, Laino L, LoMuzio L. Biological and Therapeutic Activities and Anticancer Properties of Curcumin', *Experimental and Therapeutic Medicine*. 2015; 10(5): 1615-1623.
 7. Nelson KM, Dahlin JL, Bisson J, Graham J, Pauli GF, Walters MA. The Essential Medicinal Chemistry of Curcumin. *J Med Chem*, 2017; 60(5): 1620-1637.
 8. Rachmawati H, Shaal LA, Müller RH, Keck CM. Development of Curcumin Nanocrystal: Physical Aspects. *J Pharm Sci*, 2013; 102(1): 204-214.
 9. Grill AE, Koniar B, Panyam J. Co-Delivery of Natural Metabolic Inhibitors in a Self-Microemulsifying Drug Delivery System for Improved Oral Bioavailability of Curcumin. *Drug Deliv Transl Res*, 2014; 4(4): 344-352.
 10. Chen YZ, Zhang R, Jiao L, Jiang HL. Metal–Organic Framework-Derived Porous Materials for Catalysis. *Coord Chem Rev*, 2018; 362: 1-23.
 11. Mason JA, Veenstra M, Long JR. Evaluating Metal–Organic Frameworks for Natural Gas Storage. *Chem Sci*, 2014; 5(1): 32-51.
 12. Cai W, Wang J, Chu C, Chen W, Wu C, Liu G. Metal–Organic Framework-Based Stimuli-Responsive Systems for Drug Delivery. *Adv Sci*, 2019; 6(1): 1801526.
 13. To TA, Vo YH, Nguyen HTT, Ha PTM, Doan SH, Doan TLH, Li S, Le HV, Tu TN, Phan NTS. Iron-Catalyzed One-Pot Sequential Transformations: Synthesis of Quinazolinones via Oxidative Csp³H Bond Activation using a New Metal–Organic Framework as Catalyst. *J Catal*, 2019; 370: 11-20.
 14. Thi Dang Y, Hoang HT, Dong HC, Bui KBT, Nguyen LHT, Phan TB, Kawazoe Y, Doan TLH. Microwave-Assisted Synthesis of Nano Hf- and Zr-Based Metal–Organic Frameworks for Enhancement of Curcumin Adsorption. *Microporous Mesoporous Mater*, 2020; 298: 110064.
 15. Tran TV, Le HTN, Ha HQ, Duong XNT, Nguyen LHT, Doan TLH, Nguyen HL, Truong T. A Five Coordination Cu(II) Cluster-Based MOF and Its Application in the Synthesis of Pharmaceuticals via sp³ C–H/N–H Oxidative Coupling. *Catal Sci Technol*, 2017; 7(16): 3453-3458.
 16. Sue YC, Wu JW, Chung SE, Kang CH, Tung KL, Wu KCW, Shieh FK. Synthesis of Hierarchical Micro/Mesoporous Structures via Solid–Aqueous Interface Growth: Zeolitic Imidazolate Framework-8 on Siliceous Mesocellular Foams for Enhanced Pervaporation of Water/Ethanol Mixtures. *ACS Appl Mater Interfaces*, 2014; 6(7): 5192-5198.
 17. Shieh FK, Wang SC, Yen CI, Wu CC, Dutta S, Chou LY, Morabito JV, Hu P, Hsu MH, Wu KCW, Tsung CK. Imparting Functionality to Biocatalysts via Embedding Enzymes into Nanoporous Materials by a de Novo Approach: Size-Selective Sheltering of Catalase in Metal–Organic Framework Microcrystals. *JACS*, 2015; 137(13): 4276-4279.
 18. Liao YT, Matsagar BM, Wu KCW. 'Metal–Organic Framework (MOF)-Derived Effective Solid Catalysts for Valorization of Lignocellulosic Biomass. *ACS Sustain Chem Eng*, 2018; 6(11): 13628-13643.
 19. Lee JH, Nguyen TT, Hoang Doan TL. Functionalization of Zirconium-Based Metal–Organic Frameworks for Gas Sensing Applications. *J Hazard Mater*, 2021; 403: 124104.
 20. Nguyen TT, Nguyen LHT, Mai NXD, Hoang Doan TL. Mild and Large-scale Synthesis of Nanoscale Metal–Organic Framework Used as a Potential Adenine-based Drug Nanocarrier. *J Drug Deliv Sci Technol*, 2021; 61: 102-135.
 21. Nguyen TT, Nguyen LHT, Mai NXD, Hoang Doan T L. Heterocyclic Reaction Inducted by Brønsted-Lewis Dual Acidic Hf-MOF under Microwave Irradiation. *Mol. Catal.*, 2021; 499: 111291.
 22. Namdeo M, Saxena S, Tankhiwale R, Bajpai M, Mohan YM, Bajpai SK. Magnetic Nanoparticles for Drug Delivery Applications. *J Nanosci Nanotechnol*, 2008; 8 (7): 3247-3271.
 23. Espallargas G, Coronado E. Magnetic Functionalities in MOFs: from the Framework to the Pore. *Chem Soc Rev*, 2018; 47(2): 533-557.
 24. Kurmoo M. Magnetic Metal–Organic Frameworks. *Chem Soc Rev*, 2009; 38(5): 1353-1379.
 25. George P, Das RK, Chowdhury P. Facile Microwave Synthesis of Ca-BDC Metal Organic Framework for Adsorption and Controlled Release of Curcumin. *Microporous Mesoporous Mater*, 2019; 281: 161-171.
 26. Nasseh N, Barikbin B, Taghavi L, Nasser MA. Adsorption of Metronidazole Antibiotic using a New Magnetic Nanocomposite from Simulated Wastewater (Isotherm, Kinetic and Thermodynamic Studies). *Compos. B. Eng*, 2019; 159: 146-156.
 27. Wu G, Ma J, Li S, Guan J, Jiang B, Wang L, Li J, Wang X, Chen L. Magnetic Copper-Based Metal Organic Framework as an Effective and Recyclable Adsorbent for Removal of Two Fluoroquinolone Antibiotics from Aqueous Solutions. *J Colloid Interface Sci*, 2018; 528: 360-371.
 28. Indriyani A, Yulizar Y, Yunarti R, Marcony R S. One-Pot green Fabrication of BiFeO₃ Nanoparticles via *Abelmoschus Esculentus* L. Leaves Extracts for Photocatalytic Dye Degradation. *Appl Surf Sci*, 2021; 563: 150113.
 29. Liu Y, Cherkasov N, Gao P, et al. The Enhancement of Direct Amide Synthesis Reaction Rate Over TiO₂@SiO₂@NiFe₂O₄ Magnetic Catalysts in the Continuous Flow under Radiofrequency Heating. *J. Catal*, 2017; 355: 120-130.
 30. Lv H, Rebrov E V, Gao P, Controllable Synthesis of One-Dimensional Isolated Ni_{0.5}Zn_{0.5}Fe₂O₄ Microtubes for Application as Catalyst Support in RF Heated Reactors. *Ceram Int*, 2016; 42: 7793-7802.
 31. Gharagozlou M. Study on the Influence of Annealing Temperature and Ferrite Content on the Structural and Magnetic Properties of x(NiFe₂O₄)/(100-x)SiO₂ Nanocomposites, *J Alloys Compd*, 2010; 495(1): 217-223.
 32. Mitra S, Mandal K, Anil Kumar P. Temperature Dependence of Magnetic Properties of NiFe₂O₄ Nanoparticles Embedded in SiO₂ Matrix. *J Magn Magn*, 2006; 306(2): 254-259.
 33. Wang H, Zhang F, Zhang W, Wang X, Lu Z, Qian Z, Sui Y, Dong D, Su W. The Effect of Surface Modification on the Morphology and Magnetic Properties of NiFe₂O₄ Nanoparticles. *J. Cryst. Growth*, 2006; 293(1): 169-174.
 34. Li Q, Li Y, Ma X, Du Q, Sui K, Wang D, Wang C, Li H, Xia Y. Filtration and Adsorption Properties of Porous Calcium Alginate Membrane for Methylene Blue Removal from Water. *Chem Eng Sci*, 2017; 316: 623-630.
 35. Mamani L, Nikzad S, Kheiri-Manjili H, Musawi S, Saeedi M, Askarlou S, Foroumadi A, Shafiee A. Curcumin-Loaded Guanidine Functionalized PEGylated I3ad Mesoporous Silica Nanoparticles KIT-6: Practical Strategy for the Breast Cancer Therapy. *Eur J Med Chem*, 2014; 83: 646-654.
 36. Yu S, Wang X, Chen Z, Wang J, Wang S, Hayat T, Wang X. Layered Double Hydroxide Intercalated with Aromatic Acid Anions for the Efficient Capture of Aniline from Aqueous

- Solution. *J Hazard Mater*, 2017; 321: 111-120.
37. Naghizadeh A, Ghafouri M. Synthesis and Performance Evaluation of Chitosan Prepared from Persian Gulf Shrimp Shell in Removal of Reactive Blue 29 Dye from Aqueous Solution (Isotherm, Thermodynamic And kinetic Study). *Iran J Chem Chem Eng*, 2017; 36(3): 25-36.
 38. Khalighi Sheshdeh R, Khosravi Nikou MR, Badii K., Yousefi Limaee N. Adsorption of Acid Blue 92 Dye On Modified Diatomite By Nickel Oxide Nanoparticles In Aqueous Solutions. *Prog Color Color Coat*, 2012; 5(2): 101-116.
 39. Azarpira H, Balarak D. Rice Husk as a Biosorbent for Antibiotic Metronidazole Removal: Isotherm Studies and Model Validation. *Int J Chemtech Res*, 2016; 9(7): 566-573.
 40. Tang L, Yu J, Pang Y, Zeng, G, Deng Y, Wang J, Ren X, Ye S, Peng B, Feng H. Sustainable Efficient Adsorbent: Alkali-Acid Modified Magnetic Biochar Derived from Sewage Sludge for Aqueous Organic Contaminant Removal. *Chem Eng Sci*, 2018; 336: 160-169.
 41. Çalışkan E., Göktürk S. Adsorption Characteristics of Sulfamethoxazole and Metronidazole on Activated Carbon. *Sep Sci Technol*, 2010; 45(2): 244-255.
 42. Kalhori EM, Al-Musawi TJ, Ghahramani E, Kazemian H, Zarrabi M. Enhancement of the Adsorption Capacity of the Light-Weight Expanded Clay Aggregate Surface for the Metronidazole Antibiotic by Coating with MgO Nanoparticles: Studies on the Kinetic, Isotherm, and Effects of Environmental Parameters. *Chemosphere*, 2017; 175: 8-20.
 43. Azizian S. Kinetic Models of Sorption: a Theoretical Analysis. *J Colloid Interface Sci*, 2004; 272 (1): 47-52.
 44. Tella AC, Owalude SO, Olatunji SJ, Adimula VO, Elaigwu SE, Alimi LO, Ajibade PA, Oluwafemi OS. Synthesis of Zinc-Carboxylate Metal-Organic Frameworks for the Removal of Emerging Drug Contaminant (Amodiaquine) from Aqueous Solution. *J Environ Sci*, 2018; 64: 264-275.
 45. Islam MM, Masum SM, Rahman MM, Molla MAI, Shaikh A, Roy S. Preparation of Chitosan from Shrimp Shell and Investigation of its Properties. *Int J Basic Appl Sci*, 2011; 11 (1):116-130.
 46. Naghizadeh A, Ghafouri M, Jafari A. Investigation of Equilibrium, Kinetics And Thermodynamics of Extracted Chitin from Shrimp Shell in Reactive Blue 29 (RB-29) Removal from Aqueous Solutions. *Desalination Water Treat*, 2017; 70: 355-363.
 47. Yao W, Yu S, Wang J, Zou Y, Lu S, Ai Y, Alharbi NS, Alsaedi A, Hayat T, Wang X. Enhanced Removal of Methyl Orange on Calcined Glycerol-Modified Nanocrystallined Mg/Al Layered Double Hydroxides. *Chem Eng J*, 2017; 307: 476-486.
 48. Manjunath SV, Kumar SM, Ngo HH, Guo W. Metronidazole Removal in Powder-Activated Carbon and Concrete-Containing Graphene Adsorption Systems: Estimation of Kinetic, Equilibrium and Thermodynamic Parameters and Optimization of Adsorption by a Central Composite Design. *J Environ Sci Health A*, 2017; 52(14):1269-1283.
 49. Ding H, Bian G. Adsorption of Metronidazole in Aqueous Solution by Fe-Modified Sepiolite. *Desalin Water Treat*, 2015; 55(6): 1620-1628.
 50. Sun L, Chen D, Wan S, Yu Z. Adsorption Studies of Dimetridazole and Metronidazole onto Biochar Derived from Sugarcane Bagasse: Kinetic, Equilibrium, and Mechanisms. *J Polym Environ*, 2018; 26(2): 765-777.
 51. Li S, Zhang X, Huang Y. Zeolitic Imidazolate Framework-8 Derived Nanoporous Carbon as an Effective and Recyclable Adsorbent for Removal of Ciprofloxacin Antibiotics from Water. *J Hazard Mater*, 2017; 321: 711-719.
 52. Masoomi MY, Morsali A. Applications of Metal–Organic Coordination Polymers as Precursors for Preparation of Nanomaterials. *Coord Chem Rev*, 2012; 256(23): 2921-2943.
 53. Manova E, Tsoncheva T, Paneva D, Rehspringer JL, Tenchev K, Mitov I, Petrov L. Synthesis, Characterization and Catalytic Properties of Nanodimensional Nickel Ferrite/Silica Composites. *Appl Catal A- Gen*, 2007; 317(1): 34-42.
 54. Guang-She L, Li-Ping L, Smith RL, Inomata H. Characterization of the Dispersion Process for NiFe₂O₄ Nanocrystals in a Silica Matrix with Infrared Spectroscopy and Electron Paramagnetic Resonance. *J Mol Struct*, 2001;560(1): 87-93.
 55. Liu XM, Fu SY, Huang CJ. Magnetic Properties of Ni Ferrite Nanocrystals Dispersed in the Silica Matrix by Sol–Gel Technique. *J Magn Magn Mater*, 2004; 281 (2): 234-239.
 56. Ma P, Zhang J, Liu P, Wang Q, Zhang Y, Song K, Li R, Shen L. Computer-Assisted Design for Stable and Porous Metal-Organic Framework (MOF) as a Carrier for Curcumin Delivery. *Lebenson Wiss Technol*, 2020; 120: 108949.
 57. Molavi H, Zamani M, Aghajanzadeh M, Kheiri Manjili H, Danafar H, Shojaei A. Evaluation of UiO-66 Metal Organic Framework as an Effective Sorbent for Curcumin's Overdose. *Appl Organomet Chem*, 2018; 32(4): e4221.
 58. Sindhu K, Rajaram A, Sreeram KJ, Rajaram R. Curcumin Conjugated Gold Nanoparticle Synthesis and its Biocompatibility. *RSC Adv*, 2014; 4(4): 1808-1818.
 59. Singh DK, Jagannathan R, Khandelwal P, Abraham PM, Poddar P. In Situ Synthesis and Surface Functionalization of Gold Nanoparticles with Curcumin and Their Antioxidant Properties: an Experimental and Density Functional Theory Investigation. *Nanoscale*, 2013; 5(5): 1882-1893.
 60. Leung HM, Harada M, Kee T. Delivery of Curcumin and Medicinal Effects of the Copper(II)-Curcumin Complexes. *Curr Pharm Des*, 2013; 19(11): 2070-2083.
 61. Huang Qi-Mao WSW, Li Qing PW, Deng PX, Zhou H, Pan ZQ. Synthesis and Characterization of Curcumin Bridged Porphyrins as Photosensitizers. *Chem J Chin Univ*, 2012; 33 (04): 732-737.
 62. Eybl V, Kotyzová D, Lešetický L, Bludovská M, Koutenský J. The Influence of Curcumin and Manganese Complex of Curcumin on Cadmium-Induced Oxidative Damage and Trace Elements Status in Tissues of Mice. *J Appl Toxicol*, 2006; 26(3): 207-212.
 63. Jiang T, Wang L, Zhang S, Sun PC, Ding CF, Chu YQ, Zhou P. Interaction of Curcumin with Al(III) and Its Complex Structures Based on Experiments and Theoretical Calculations. *J Mol Struct*, 2011; 1004: 163-173.
 64. Datmai NX, Dang YT, Kieu HTT, Doan TH, Reducing the Particle Size of Biodegradable Nanomaterial for Efficient Curcumin Loading, *J Mater Sci*, 2021; 56: 1-10.
 65. Dang YT, Dang M-HD, Mai NXD, Nguyen LHT, Phan TB, Le HV, et al. Room temperature synthesis of biocompatible nano Zn-MOF for the rapid and selective adsorption of curcumin. *Journal of Science: Advanced Materials and Devices*. 2020;5(4):560-565.